Published as: *ACS Chem Biol*. 2011 September 16; 6(9): 893–899.

Quantifying the Dynamics of Bacterial Secondary Metabolites by Spectral Multi-Photon Microscopy

Nora L. Sullivan[1,2,3], **Dimitrios S. Tzeranis**[3,4], **Yun Wang**[1,5], **Peter T.C. So**[4,6], and **Dianne Newman**[1,7,*]

[1]Department of Biology and Howard Hughes Medical Institute, Massachusetts Institute of Technology, Cambridge, MA, USA

[4]Department of Mechanical Engineering, Massachusetts Institute of Technology, Cambridge, MA, USA

[6]Department of Biological Engineering, Massachusetts Institute of Technology, Cambridge, MA, USA

Abstract

Phenazines, a group of fluorescent small molecules produced by the bacterium *Pseudomonas aeruginosa*, play a role in maintaining cellular redox homeostasis. Phenazines have been challenging to study *in vivo* due to their redox activity, presence both intra- and extracellularly, and their diverse chemical properties. Here, we describe a non-invasive *in vivo* optical technique to monitor phenazine concentrations within bacterial cells using time-lapsed spectral multi-photon fluorescence microscopy. This technique enables simultaneous monitoring of multiple weakly-fluorescent molecules (phenazines, siderophores, NAD(P)H) expressed by bacteria in culture. This work provides the first *in vivo* measurements of reduced phenazine concentration as well as the first description of the temporal dynamics of the phenazine-NAD(P)H redox system in *Pseudomonas aeruginosa*, illuminating an unanticipated role for 1-hydroxyphenazine. Similar approaches could be used to study the abundance and redox dynamics of a wide range of small molecules within bacteria, both as single cells and in communities.

Small molecules play a variety of roles for microorganisms, including serving as cofactors within proteins, acting as antibiotics, functioning as inter- and intra-cellular signals, and facilitating iron uptake (1). Given their widespread importance (2), the development of novel methods to measure them *in vivo* has been recognized as a research priority (3). Due to their small size and varied structures, studying the physiological functions of small molecules is quite challenging. Standard biochemical techniques quantify the amount of small molecules released by a bacterial population by purifying individual components from cultures (4) or measuring small molecule activity (5). Such techniques have limited time resolution and often cannot identify modifications including changes in redox state. These limitations can be circumvented when studying fluorescent small molecules because their spatio-temporal expression can be quantified by fluorescence microscopy and spectroscopy. As proof of principle, we utilized spectral multi-photon microscopy to study several fluorescent small molecules (phenazines, NAD(P)H) in the opportunistic pathogen

*dkn@caltech.edu.
[2]current address: Molecular and Cellular Biology Department, Harvard University, Cambridge, MA, USA
[3]These authors contributed equally to this work.
[5]current address: Department of Civil and Environmental Engineering, Northwestern University, Evanston, IL USA
[7]current address: Division of Biology and Howard Hughes Medical Institute, California Institute of Technology, Pasadena, CA, USA

Supporting Information Available: This material is available free of charge *via* the Internet.

Pseudomonas aeruginosa. While biochemical studies usually focus on one or a few time-points, fluorescence microscopy provides the ability to quantify multiple fluorescent components over long periods of time with fast temporal sampling, and acquire information about the underlying molecular circuitry based on the temporal response of each component when the circuitry is manipulated. Here, we describe a sensitive imaging technique to measure the impact of phenazines on the redox state of *P. aeruginosa* under O_2-limited conditions.

The wild type *P. aeruginosa* strain PA14 produces several fluorescent small molecules: the two redox-active co-factors NAD(P)H and FAD, which are fluorescent in their reduced and oxidized states, respectively (6); the two iron siderophores pyoverdine (PVD) and pyochelin (PCH) (7); and finally phenazines, a group of redox-active secondary metabolites. *P. aeruginosa* produces several kinds of phenazines: the precursor phenazine-1-carboxylic acid (PCA), 1-hydroxyphenazine (1OHP), pyocyanin (PYO), 5-methyl-phenazine-1-carboxylic acid (5MPCA), and phenazine 1-carboxamide (PCN) (Figure 1a,b; Figure 2b) (8). Phenazines are produced and reduced by bacterial cells and are oxidized extracellularly by terminal electron acceptors including Fe(III) and O_2 (9); their intracellular reduction has been implicated in facilitating redox homeostasis (4) and survival (10) when cells are oxidant-limited.

Each phenazine can exist in two stable redox states. The oxidized phenazines PCA_{ox}, PYO_{ox}, $1OHP_{ox}$ are non-fluorescent. Reduction of these phenazines by the addition of two electrons and two hydrogen ions changes their color and converts them into the fluorescent molecules PCA_{red}, PYO_{red}, $1OHP_{red}$ (Figure 1a). PCN, on the other hand, is fluorescent in both its oxidized and reduced form, while 5MPCA is only fluorescent when oxidized. We neglected the fluorescence emission of FAD_{ox} and PCN_{red} because these fluorophores are excited inefficiently by our system. Experimentally observed concentrations of phenazines released by *P. aeruginosa* in culture depend on the bacterial strain and the culture conditions. The maximal published measurement of extracellular concentration of PYO in stationary cultures is 275 μM (4).

The ability of reduced phenazines to fluoresce makes it possible to monitor their concentration *in vivo* by fluorescence microscopy directly without end-point extraction. Because reduced phenazines are weak fluorophores, accurate quantification requires sensitive instrumentation in order to minimize cell damage. We imaged several *P. aeruginosa* strains in suspension by two-photon excitation microscopy (TPEM) and took advantage of TPEM's high sensitivity, low noise levels, and low level of cellular photo-damage (11). TPEM imaging of intrinsic fluorophores (most commonly NAD(P)H and FAD) has been applied to mammalian cells to quantify their metabolic state (12), and has found several applications that range from an analysis of blood flow and oxygen diffusion in the mouse brain (13) to identification of precancerous cells (14). While mammalian cell metabolism has been studied extensively, a similar fluorescence-based approach has not previously been applied to study bacterial metabolism. The presence of several fluorescent small molecules related to *P. aeruginosa* redox state (phenazines, siderophores, cofactors) provides an opportunity to probe the molecular circuitry that regulates the redox state of *P. aeruginosa*. At the same time, the presence of multiple weak fluorophores of similar emission spectra (see Figure 1) makes the separation of the emissions of the individual components challenging.

To distinguish the emissions of the fluorescent components in our samples, we imaged P. aeruginosa using a 16-channel spectral multi-photon microscope. Specifically, the microscope was equipped with a spectrally resolved detector comprising a spectrograph and a 16-channel photomultiplier tube (PMT). Each channel of the PMT detects the emission

spectrum within a 13 nm band. The acquired 16-channel spectrum of each pixel was subsequently analyzed using a maximum-likelihood calculation to estimate the contribution of each fluorophore to the detected signal. Initially, we characterized the excitation and emission fluorescence spectra of the fluorescent small molecules found in *P. aeruginosa* using both single-photon and two-photon excitation (Figure 1c,d,e,f). The single-photon excitation and emission spectra (Figure 1c,d) of each phenazine was measured using a spectrophotometer inside an anaerobic chamber. The two-photon action cross-section and emission spectrum (Figure 1e,f) of each compound were measured from aqueous solutions anaerobically sealed inside well slides using the spectral multi-photon microscope. Phenazines' two-photon cross sections are similar and approximately 40 times smaller than PVD and 400 times smaller than fluorescein (Figure 1e). Although the single-photon and two-photon measurements have different sampling intervals (1 nm and 13 nm respectively), data show that the emission spectra of PYO_{red}, $1OHP_{red}$, PVD, and NAD(P)H do not depend on the method of excitation (single photon or two-photon) similar to the vast majority of fluorophores (Figure 1d,f). However, the two-photon emission spectrum of PCA_{red} is approximately 20 nm blue-shifted compared to its single-photon emission spectrum. This observed shift is not fully elucidated but may be attributed to PCA_{red} having heterogeneous ground states, with different one- and two-photon absorption cross sections, coupled to excited states with different emission spectra.

To quantify the concentration of reduced phenazines in *P. aeruginosa* and also to quantify the effect of different phenazines on the redox state of NAD(P)H, we imaged several *P. aeruginosa* strains over a period of 90 minutes after transferring the cells from an O_2-rich stationary phase culture to an O_2-limited environment (see Methods). Each strain produces a unique assortment of the fluorescent small fluorescent molecules (Figure 2a). The wild-type PA14 strain can produce all the endogenous fluorophores considered in this study. The mutant strains contained clean deletions in the pyocyanin biosynthesis gene (Δ*phzM*), or phenazine (Δ*phz1/2*) or siderophore (Δ*pvdA*Δ*pchE*, referred to as Δ*sid*) biosynthesis genes, or both (Δ*phz1/2*Δ*sid*), resulting in no production of the respective fluorescent molecules (Figure 2a,b).

As expected, the fluorescence emission of the phenazine-producing strains (PA14, Δ*phzM*, Δ*sid*) had a larger magnitude than the phenazine-null strains (Δ*phz1/2*, Δ*phz1/2*Δ*sid*) (Figure 2c). The largest part of the detected signal in the wild-type (PA14) strain and the siderophore mutant (Δ*sid*) strain appeared to be emitted by PYO_{red}, and, to a lesser extent, by PCA_{red} and NAD(P)H (Figure 2c). The primary contributor to the emission of the phenazine-null strains (Δ*phz1/2*, Δ*phz1/2*Δ*sid*) was NAD(P)H (Figure 2b). The PVD fluorescence was indistinguishable from background in all strains likely due to the low concentrations of PVD produced by the cells in the iron-rich growth medium and to iron-mediated quenching of any PVD present. We initially considered only the major known endogenous fluorophores in our analysis (PCA_{red}, PYO_{red}, NAD(P)H, PVD), and found that although the fitting error in all phenazine-producing strains was on the order of 10-15% RMS, the fitting error in the Δ*phzM* strain was substantially larger (≥25% RMS). Our data revealed that although this strain cannot produce PYO_{red}, there was significant fluorescence emission (above background) around the PYO_{red} emission peak and the fitting error was significantly reduced by including a component with PYO_{red}–like emission (Figure 2d). Furthermore, the estimated contribution of this PYO_{red}–like emission starts at the background noise level and increases in an exponential-like manner with time dynamics similar to the ones observed for PYO_{red} in PYO-producing strains (Figure 3a,b). Because the Δ*phzM* strain produces the precursor PCA and can convert PCA to other phenazines (except PYO) (Figure 2b), it is likely that the PYO_{red}-like emission could originate from another phenazine. Although the red phenazine (5MPCA) has been shown to accumulate in the Δ*phzM* strain (15), 5MPCA is fluorescent in its oxidized form and its emission peak is

quite different from our unknown component (620 nm vs 490 nm). It is unlikely, therefore that the unknown detected compound is 5MPCA. However, the unknown detected compound could be the less-studied $1OHP_{red}$, which has an emission spectrum very similar to PYO_{red} (Figure 1d,f). In this case, due to the similarity of the emission spectra of PYO_{red} and $1OHP_{red}$, it is not possible to resolve the signal emitted by these two fluorophores. After background correction, the total PYO_{red}-like emission of the Δ*phzM* strain (which can express $1OHP_{red}$ but not PYO_{red}) starts at the noise level and reaches a steady state fluorescence emission of approximately 200 μM $1OHP_{red}$, which is equivalent to the emission emitted by 100 μM PYO_{red}. Additionally, although it is possible that *P. aeruginosa* produces fluorescent molecules that are not considered in this study, we believe that any possible contribution by these components is negligible for the following reasons. 1) We have characterized (Figure 1) or discussed (FAD, PCN, PCH, and 5MPCA) all the known fluorescent molecules produced by each *P. aeruginosa* strain. 2) In all strains, the detected emission can be consistently well approximated as a sum of the emission of the fluorophores known to be produced by each strain (Figure 2a). 3) Furthermore, no region of the spectrum contains a consistently large fitting error which would suggest the presence of an additional fluorophore (as was the case when 1OHPhz emission was omitted in the Δ*phzM* strain (Figure 2d)). Therefore, while it is possible that a small fraction of the overall fluorescent signal could come from compounds not considered in this analysis, their presence would not affect significantly our calculations and would not impact our conclusions.

The detected fluorescent emission of most fluorophores shows significant variation over the time course of the experiment (90 minutes). This change cannot be attributed to photo-bleaching: at each time point the fluorophore emission of each strain was determined by imaging four different random cell populations briefly (125 μsec per pixel) at conditions that did not cause photo-bleaching in solutions of pure fluorophores *in vitro* (see methods). The time response of the estimated fluorescent component concentration (with the exception of NAD(P)H in phenazine-null strains) show a similar temporal pattern, increasing from its initial concentration to a different steady-state concentration in a way that fit well to single-order exponential functions, whose time constant lies between 16 and 25 min (Figure 3a,b). In all phenazine-producing bacteria (PA14, Δ*phzM*, and Δ*sid*) the concentration of PCA_{red} increased at least two-fold from its initial concentration to a steady-state concentration. In both PYO-producing bacteria (PA14 and Δ*sid*) the intracellular concentration of PYO_{red} increased at least 10-fold from a similar initial low concentration to a steady-state concentration. The observed increase of PCA_{red} and PYO_{red} concentration in strains PA14, Δ*phzM*, and Δ*sid* is consistent with the low availability of O_2 in the imaging environment. Concomitantly, the concentration of NAD(P)H in all phenazine-producing strains exponentially decreased from a high initial concentration to a lower steady state concentration. In the Δ*phz1/2* and Δ*phz1/2*Δ*sid* mutants, the concentration of NAD(P)H remained constant, consistent with phenazines being electron carriers and redox state modulators (1, 4, 15, 16). This is further supported by the observation that the two strains that produce PYO (the phenazine that reacts most readily with O_2) (9), showed similar NAD(P)H responses. Finally, while the lack of phenazines dramatically altered the time response of NAD(P)H, the absence of PVD had negligible effects (PA14 vs Δ*sid* or Δ*phz1/2* vs Δ*phz1/2*Δ*sid*). This is logical given that PVD is not redox active and the medium is iron rich (which would disfavor PVD production).

Interestingly, the concentrations of PCA_{red} and PYO_{red} at all time points were positively linearly correlated for all three phenazine-producing strains, suggesting that PCA_{red} and PYO_{red} interact by some mechanism whose dynamics are much faster than the sampling period of our experiments. The PCA_{red} vs PYO_{red} plot (Figure 3c) shows that the linear correlation between PCA_{red} and PYO_{red} is very similar in strains PA14 and Δ*sid* but the slope is different in strain *phzM* where the PYO_{red}-like signal is likely contributed by the

phenazine $1OHP_{red}$. We therefore believe that the interactions between these phenazines are specific for the particular molecules and might be due to inter-conversion between the two chemical species and/or a redox interaction. The strong inverse linear correlation between PCA_{red} (and/or PYO_{red}) and NAD(P)H indicates that these two redox active molecules interact directly or indirectly. Previous studies have demonstrated that as *P. aeruginosa* enters stationary phase, O_2 in the medium becomes undetectable and the bulk intracellular $NADH/NAD^+$ ratio increases (4). While the NADH level remains high in the Δ*phz1/2* strain, the production of phenazines by the wild type or the addition of exogenous phenazines to the mutant result in a decrease in the $NADH/NAD^+$ ratio (4). The analysis of our imaging data confirmed this, and provides direct evidence for the role of phenazines in redox homeostasis. However, the growth and assay conditions used in the two studies were substantially different, precluding a direct comparison. Because NAD(P)H is capable of phenazine reduction *in vitro* (17), the inverse linear relationship seen here is likely a result of the redox reaction between these two species. However, because NADH is also required for phenazine biosynthesis (8), the decline in the NAD(P)H pool could correlate with an increase in the total phenazine population rather than just the reduced fraction.

To our knowledge, these measurements provide the first estimation of the intracellular concentration of reduced phenazines, and the first description of phenazine redox dynamics *in vivo*. Encouragingly, the reduced phenazine concentrations estimated through fluorescence microscopy were similar to those obtained in parallel using standard biochemical extraction methods: for strains PA14, Δ*phzM*, and Δ*sid* the initial cell-associated PCA_{total} was 17.6 ± 14.6 μM, 92.4 ± 4.9 μM, and 7.7 ± 0.8 μM, respectively, and the concentration of cell-associated PYO_{total} was 79.6 ± 0 μM and 61.9 ± 5.9 μM, respectively. Both estimations of phenazine concentrations (optical measurements and biochemical extractions) are approximations of the true cellular concentrations because sample preparation steps (including centrifugation, cell resuspension) and O_2 exposure during the manipulations impact the values determined by either technique.

In summary, the spectral multi-photon microscopy imaging method described here has broad application for the *in vivo* imaging of multiple fluorescent metabolites within living microbial cells. In the case of phenazines and *P. aeruginosa*, controlled perturbation of the phenazine concentration in the cellular environment coupled to monitoring the response would enhance our understanding of how phenazines control the behaviors of microbial communities in time and space. Looking beyond *P. aeruginosa*, we anticipate that this approach could also be applied to quantify the redox dynamics of multiple endogenous or induced fluorescent molecules in bacteria and other organisms.

METHODS

All bacterial strains and culture conditions, methods for phenazine extraction and quantification, and the custom two-photon microscope set-up are described in Supporting Information.

Imaging Conditions for Standards

The single-photon emission spectrum of phenazines was measured using a spectrophotometer inside an anaerobic chamber at 1 nm intervals. The two-photon excitation spectrum was measured inside anaerobically sealed well slides using the two-photon microscope described in Supporting Information. Sealed well slides were made using well slides (Aquatic Eco-Systems) with a pair of 1 mm holes drilled in the well (Ferro Ceramics). The open surface was then covered by a coverslip (VWR) and sealed with heat-sealing film (Solaronix) using a soldering iron. Slides were incubated for at least 3 days in an anaerobic chamber prior to use. At time of use, the chamber in the slide was filled with ~40 μl of the

standard using the holes and then covered and sealed with another coverslip and sealing film. To minimize any oxygen leakage in these compartments, the samples were imaged as quickly as possible following removal from the anaerobic chamber.

Single-photon and two-photon emission spectra measurements took place under the same buffer conditions (50 mM MOPS pH 7.2 for phenazines, PBS pH 7.4 for PVD and NADH). The single-photon and two-photon emission spectra measurements are slightly different due to the different sampling methods used by the two instruments. For two-photon emission spectrum measurements, the emission is resolved optically in a diffraction grating and then detected by a 16-channel photomultiplier tube. Therefore, the measurement of each channel integrates the emission spectrum within a 13 nm region of the spectrum. For single-photon emission spectrum measurements, a monochromator is used to sample the emission around a particular wavelength. The calculation of the two-photon cross sections was done according to the method described in (18). Briefly, the two-photon cross-section - quantum yield product of each compound was calculated indirectly by imaging and comparing with the known two-photon cross-section - quantum yield product of fluorescein.

We observed a difference in the emission spectra of PCA after one-photon and two-photon excitation. This difference cannot be attributed to the differential sensitivity of the sensors used for the single-photon and two-photon measurements: although PCA and orange fluorescent beads (Invitrogen F8820) have similar single-photon emission spectra peaks, their two-photon emission spectra differ (Supplementary Figure 1).

Bacteria Two-Photon Imaging

Each bacterial strain was grown to stationary phase overnight. 1 ml of culture was concentrated 20× in PBS (to remove background fluoresence emitted by the growth medium), and mounted in a 40 μl-well covered by a sealed coverslip (as described above, but without the second coverslip). These conditions result in an oxygen limited environment for the bacteria trapped inside the sealed well. Four spatially resolved images of each sample were taken at approximately 4, 12, 20, 25, 40, and 90 minutes after transferring the bacteria into the sealed coverslip.

Data Analysis

Since the mean number of detected photons per bacterial pixel was quite low (approximately 5-10), the estimation of the average concentration of each fluorescent component in each bacterial strain was accomplished in three steps: 1) Pixel classification: image pixels were classified as “bacteria” or “medium” based on the known background noise emission, (Supplementary Figure 2). 2) Signal decomposition: The 16-channel photon counts of all “bacterial” pixels were summed into one “super-pixel”. The photon contribution of each fluorescent component (reduced phenazines, PVD, and NADH) to the total photon count y of this super-pixel is estimated by a maximum-likelihood calculation based on the distinct emission spectra of the fluorophores. 3) Convert into equivalent fluorophore concentration: The mean photon emission per bacterium pixel for each component is converted into equivalent fluorophore concentration via a concentration-emission standard curve.

The objective of the signal decomposition step was given the photon emission of bacterial pixels $\underline{y}$ to calculate the maximum-likelihood estimate (MLE) of the poisson emission rate of each compound $_{\lambda}i$. The MLE of the rate vector $\underline{\lambda} = [\lambda_1 \ldots \lambda_N]^T$ was found by maximizing the observation likelihood:

$$\ln\left(p_{\underline{Y};\underline{\Lambda}}\left(\underline{y};\underline{\lambda}\right)\right)=\sum_{i=1}^{N}\lambda_i+\sum_{j=1}^{16}\frac{\left(\underline{t}^{T}{}_{j}\underline{\lambda}\right)^{-y_j}}{y_j!}$$

where y_j is the detected photon count in channel j, $\underline{t}^{T}{}_{j}$ is the j-th row of the spectral matrix $\underline{S}$ (the matrix whose columns correspond to the normalized (sum of elements equal 1) emission spectra of the fluorescent components). The fluorescent spectra $\underline{s}_i$ of the compounds were determined by imaging pure compounds. It was assumed that the emission spectra $\underline{s}_i$ of phenazines and PVD *in vivo* are identical to the ones of the pure compounds. For simplicity, it was also assumed that 80% NADH is bound to proteins (based on previous *in vivo* findings (6)). As initial guess of the MLE calculation was chosen the non-negative least-squares solution (19) of the linearized problem (where the emission is assumed to be a linear sum of the signals emitted by each fluorophore (Figure 2b) $\underline{y}=\underline{S}\cdot\underline{\lambda}$. To avoid overfitting, for each bacteria strain data decomposition considered only the fluorophores known to be expressed in this strain plus one extra component that describes the channel-dependent background noise (includes dark current noise and stray light noise). The average signal per bacterial pixel for each compound was then estimated by dividing the total photon contribution of each compound by the number of bacterial pixels. All images were found to contain similar level of background noise (about 0.2 photons per pixel) which agrees with instrument calibration data taken on blank (PBS) samples. As an additional control, when all fluorophores are considered in the signal decomposition calculation, the photon emission assigned to fluorophores not present in the strain was equal or less to background noise level.

In order to convert the MLE of the emission rate λ_i of each fluorescent compound into an equivalent compound concentration, it was assumed that the emission rate λ_i of each fluorophore is analogous to its concentration c_i through a proportionality constant called brightness $b_i=\lambda_i/c_i$ (photon counts per pixel per time per unit concentration per laser power). The brightness of each fluorescent compound was determined experimentally, by measuring three solutions of known concentrations (50, 100, 500 μM) under acquisition conditions (laser power, sampling time) identical to the conditions of the bacteria imaging experiment. The brightness corresponds to the slope of the resulting fluorophore concentration versus the detected emission curve. For all components, results suggested that the experimental conditions did not result in fluorophore saturation or fluorophore photobleaching (the detected photon count was analogous to the fluorophore concentration and analogous to the square power of the laser power; repeated measurements on the same sample over a period of half an hour provided consistent results). Because the brightness of a fluorophore is analogous to its two-photon cross section, our calculations assume that the two-photon cross section of the fluorophores *in vivo* are identical to the ones of the pure compounds

Imaging and estimation of fluorophore concentration $c(t)$ took place between t=4 min and t=90 min after transferring the bacteria into the oxygen-limiting environment of the sealed coverslip. The time response $c(t)$ of each fluorophore's intracellular concentration was then fitted to the exponential curve $c(t)=c_{ss}+(c_0-c_{ss})\cdot\exp(-t/\tau)$, by nonlinear least square. c_0 is the initial value of the fluorophore concentration at t=0, c_{ss} is the steady state fluorophore concentration, and τ is the time constant of the fluorophore concentration response. The initial value c_0 approximates the fluorophore concentration in the stationary culture because our results show that reduced phenazine/NADH dynamics are much slower than 4 minutes (the time constant τ of intracellular reduced phenazine/NADH was found to be larger than 15 minutes, Figure 3b).

Supplementary Material

Refer to Web version on PubMed Central for supplementary material.

Acknowledgments

We thank L. Dietrich for the gift of the Δ*phzM* strain, and A. Price-Whelan and L. Dietrich for helpful advice and discussions. DKN is a Howard Hughes Medical Institute Investigator, and this work was supported by the HHMI. DST and PTCS were supported by NIH, NSF, SMA2, and SMART.

References

1. Price-Whelan A, Dietrich LE, Newman DK. Nat Chem Biol. 2006; 2:71–8. [PubMed: 16421586]
2. Straight PD, Kolter R. Annu Rev Microbiol. 2009; 63:99–118. [PubMed: 19566421]
3. Council, NR. Research at the Intersection of the Physical and Life Sciences. National Academies Press; Washington DC: 2010.
4. Price-Whelan A, Dietrich LE, Newman DK. J Bacteriol. 2007; 189:6372–81. [PubMed: 17526704]
5. Xavier KB, Bassler BL. J Bacteriol. 2005; 187:238–48. [PubMed: 15601708]
6. Chance B. Science. 1954; 120:767–75. [PubMed: 13216168]
7. Elliott RP. Appl Microbiol. 1958; 6:241–6. [PubMed: 13559972]
8. Mavrodi DV, Bonsall RF, Delaney SM, Soule MJ, Phillips G, Thomashow LS. J Bacteriol. 2001; 183:6454–65. [PubMed: 11591691]
9. Wang Y, Newman DK. Environ Sci Technol. 2008; 42:2380–6. [PubMed: 18504969]
10. Baron SS, Rowe JJ. Antimicrob Agents Chemother. 1981; 20:814–20. [PubMed: 6798928]
11. Dietrich LE, Teal TK, Price-Whelan A, Newman DK. Science. 2008; 321:1203–6. [PubMed: 18755976]
12. Schwarzer C, Fischer H, Kim EJ, Barber KJ, Mills AD, Kurth MJ, Gruenert DC, Suh JH, Machen TE, Illek B. Free Radic Biol Med. 2008; 45:1653–62. [PubMed: 18845244]
13. Denk W, Strickler JH, Webb WW. Science. 1990; 248:73–6. [PubMed: 2321027]
14. Skala MC, Riching KM, Gendron-Fitzpatrick A, Eickhoff J, Eliceiri KW, White JG, Ramanujam N. Proc Natl Acad Sci U S A. 2007; 104:19494–9. [PubMed: 18042710]
15. Kasischke KA, Lambert EM, Panepento B, Sun A, Gelbard HA, Burgess RW, Foster TH, Nedergaard M. J Cereb Blood Flow Metab. 2011; 31:68–81. [PubMed: 20859293]
16. Bird DK, Yan L, Vrotsos KM, Eliceiri KW, Vaughan EM, Keely PJ, White JG, Ramanujam N. Cancer Res. 2005; 65:8766–73. [PubMed: 16204046]
17. Dietrich LE, Price-Whelan A, Petersen A, Whiteley M, Newman DK. Mol Microbiol. 2006; 61:1308–21. [PubMed: 16879411]
18. Kito N, Ohnishi Y, Kagami M, Ohno A. Chemistry Letters. 1974:353–356.
19. Albota MA, Xu C, Webb WW. Appl Opt. 1998; 37:7352–6. [PubMed: 18301569]
20. Lawson, CL.; H. R. J.. Solving least squares problems. Prentice-Hall; Englewood Cliffs, N.J.: 1974.
21. Buehler C, Kim KH, Greuter U, Schlumpf N, So PT. J Fluoresc. 2005; 15:41–51. [PubMed: 15711876]
22. Rahme LG, Stevens EJ, Wolfort SF, Shao J, Tompkins RG, Ausubel FM. Science. 1995; 268:1899–902. [PubMed: 7604262]

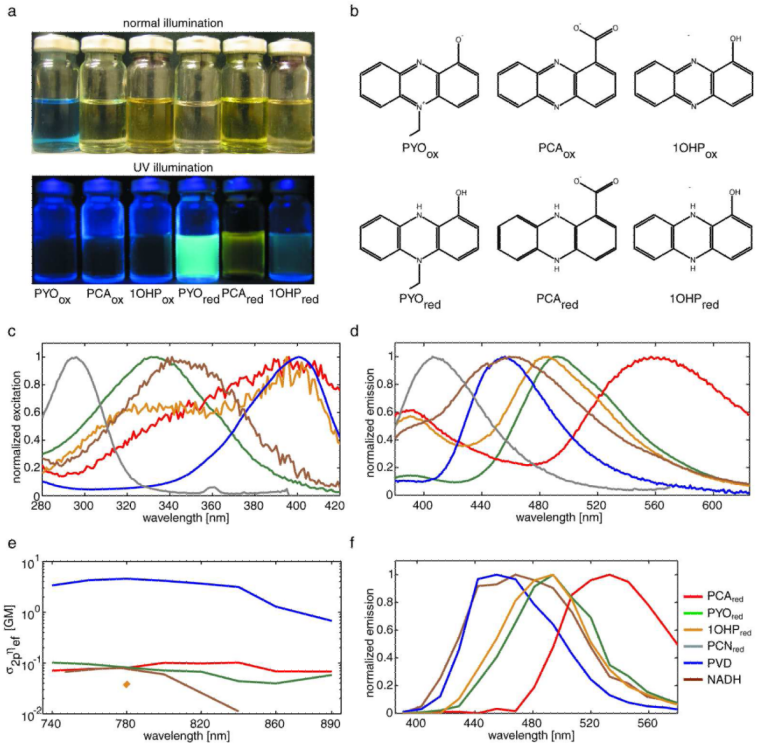

Figure 1.

Characterization of one- and two-photon excitation fluorescence spectroscopic properties of phenazines. a) Images of oxidized and reduced phenazine samples under normal (top) and UV illumination (bottom). b) Chemical structures of oxidized and reduced phenazines. c) Single-photon excitation spectra of phenazines (PCA_{red}, PYO_{red}, $1OHP_{red}$), NADH and PVD. d) Emission spectra of phenazines, NADH and PVD after single-photon excitation, taken at 1nm spacing. e) Two-photon cross-sections of phenazines, NADH and PVD. f) Emission spectra of phenazines, NADH and PVD after two-photon excitation, as detected by a 16-channel sensor that integrated spectra over 13 nm intervals.

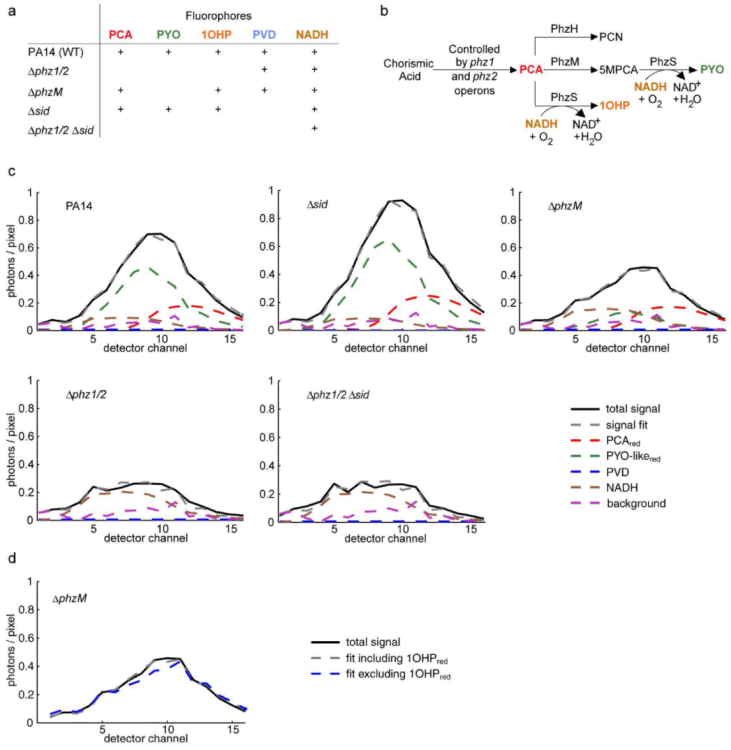

Figure 2.

Characterizing the endogenous fluorescent molecules present in *P. aeruginosa*. a) Identity of the fluorescent components produced by each strain used in the study. b) Biosynthesis pathway of the phenazines produced by *P. aeruginosa*. Genes and gene products responsible for each conversion are listed above the arrows (8). c) Representative examples of the measured 16-channel fluorescent spectra from the five bacterial strains at t=90 min (solid line) and non-negative least square estimations of the contributions of each strain's fluorescent components (dashed lines)

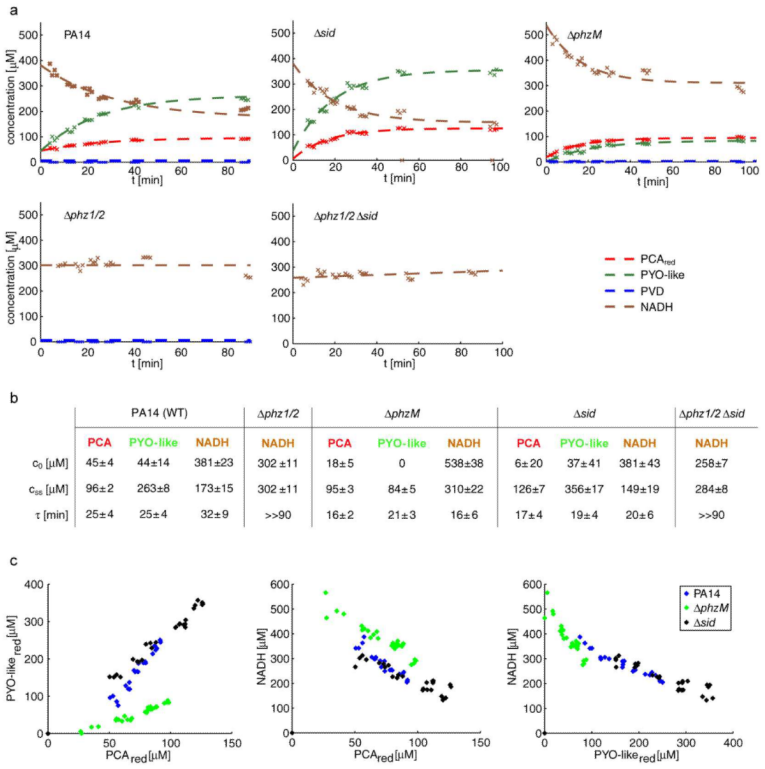

Figure 3.

Monitoring the *in vivo* response of *P. aeruginosa* to a sudden change in the available oxygen (t=0 min) by two-photon imaging of intracellular reduced phenazines and NADH. a) Time response (0 to 90 min) of the estimated concentration of the fluorescent components of each strain and fits to exponential curves. b) 95% regions of confidence for the parameters of the first order exponentials $c(t) = c_{ss} + (c_0 - c_{ss}) \cdot \exp(-t/\tau)$ used to approximate the dynamics of fluorescent components. c) Plots of the estimated PCA_{red}, PYO_{red} and NADH in the three phenazine-producing *P. aeruginosa* strains. Each point corresponds to the estimated concentration of the fluorescent components at one time instant.